energies

MDPI

Article

Rockburst Intensity Level Prediction Method Based on FA-SSA-PNN Model

Gang Xu [1,2], Kegang Li [1,2,*], Mingliang Li [1,2], Qingci Qin [1,2] and Rui Yue [1,2]

[1] School of Land and Resources Engineering, Kunming University of Science and Technology, Kunming 650093, China; 20202201005@stu.kust.edu.cn (G.X.); 20182101079@kust.edu.cn (M.L.); qqc1457186548@126.com (Q.Q.); yr@stu.kust.edu.cn (R.Y.)

[2] Yunnan Key Laboratory of Sino-German Blue Mining and Utilization of Special Underground Space, Kunming 650093, China

* Correspondence: 20070001@kust.edu.cn

Abstract: To accurately and reliably predict the occurrence of rockburst disasters, a rockburst intensity level prediction model based on FA-SSA-PNN is proposed. Crding to the internal and external factors of rockburst occurrence, six rockburst influencing factors (σ_θ, σ_t, σ_c, σ_c/σ_t, σ_θ/σ_c, W_{et}) were selected to build a rockburst intensity level prediction index system. Seventy-five sets of typical rockburst case data at home and abroad were collected, the original data were preprocessed based on factor analysis (FA), and the comprehensive rockburst prediction indexes, CPI_1, CPI_2, and CPI_3, obtained after dimensionality reduction, were used as the input features of the SSA-PNN model. Sixty sets of rockburst case data were extracted as the training set, and the remaining 15 sets of rockburst case data were used as the test set. After the model training was completed, the model prediction results were analysed and evaluated. The research results show that the proposed rockburst intensity level prediction method based on the FA-SSA-PNN model has the advantages of high prediction accuracy and fast convergence, which can accurately and reliably predict the rockburst intensity level in a short period of time and can be used as a new method for rockburst intensity level prediction, providing better guidance for rockburst prediction problems in deep rock projects.

Keywords: rock mechanics; factor analysis; sparrow search algorithm; probabilistic neural network; rockburst intensity level prediction

Citation: Xu, G.; Li, K.; Li, M.; Qin, Q.; Yue, R. Rockburst Intensity Level Prediction Method Based on FA-SSA-PNN Model. *Energies* **2022**, *15*, 5016. https://doi.org/10.3390/en15145016

Academic Editors: Marcin Kamiński and Mateus Mendes

Received: 25 May 2022
Accepted: 6 July 2022
Published: 8 July 2022

1. Introduction

Rockburst is a deep underground rock construction process of hard and brittle surrounding rock due to excavation, mining, or other external disturbances, triggered by the rapid and violent release of the elastic properties gathered in the rock and leads to the production of surrounding rock fragments by bursting, rapid ejection, or throwing the dynamic destabilization phenomenon, which are sudden, random, and extremely hazardous geological hazards [1–3]. In recent years, with the reduction of shallow mineral resources, more and more underground rock works are moving deeper at an unprecedented rate, and the rockburst hazards problem is becoming increasingly prominent. These hazards have been a pressing problem in deep underground rock engineering, often causing huge losses to construction personnel, equipment, and buildings, which in turn seriously affects the construction process, so it is particularly important to accurately predict the occurrence of rockburst hazards. Accurate and reliable prediction of rockburst hazards effectively avoids and controls rockbursts, and rockburst prediction has become a hot spot for research in the field of deep underground rock engineering [4].

In order to accurately predict the intensity level of rockburst, many experts and scholars at home and abroad have carried out exploratory research on rockburst prediction methods, which can be classified into three categories: The first category is the acoustic emission technique [5], microseismic observation technique [6], and other methods of

rockburst prediction based on field measurements; the second category is a single-factor prediction method, where the discrimination of rockburst intensity levels varies slightly with the criterion, such as Hoek criterion [7], N-Jhelum criterion [8], Erlang Mountain criterion [9], and Lujiayou criterion [10], etc. With the continuous research on the problem of rockburst prediction, a large number of scholars have gradually realized the complexity of the mechanism of rockburst and the many factors that induce rockburst [11–13], but it is difficult to accurately predict rockburst using only single-factor prediction methods. At present, non-linear theory uses more than just the third category of rockburst prediction methods, that is, the multi-factor integrated prediction method and the multi-factor integrated prediction method, to integrate rock mechanics parameters and a variety of rockburst criterion to achieve rockburst intensity level prediction. The multi-factor integrated prediction method, according to the different non-linear theory, is divided into two subcategories. The former is mainly based on mathematical methods to predict the rockburst intensity level, which are representative of ideal point method [14], cloud model theory [15,16], fuzzy comprehensive evaluation method [17–19], uncertainty measurement theory [20], gray system theory [21], the TOPSIS method [22], discriminant by distance method [23], and the extenics theory [3]. The latter is mainly based on intelligent algorithms to predict rockburst intensity levels, such as self-organizing feature mapping neural networks [24], machine learning [25,26], deep neural networks [27], generalized regression neural networks [28], and sarticle swarm optimization [29].

All of the above rockburst prediction methods have achieved some success, enriching the theory of rockburst prediction. However, there are still some shortcomings, for example, when ignoring the impact of correlation between rockburst prediction indicators on the prediction results, due to the diversity of factors affecting the occurrence of rockburst, there is a certain correlation between rockburst prediction indicators, which will not only lead to double calculation of indicators, increasing the workload in the prediction process, but will directly affect the accuracy and reliability of the prediction results. Therefore, the elimination of correlation between indicators is the key to accurate prediction of rockbursts, and research on the elimination of correlation between rockburst prediction indicators is necessary.

Factor analysis (FA) [30] is the extension and development of principal component analysis, which regroups the information of the original variables to find out the common factors affecting the variables and can make the factor variables more interpretable and give high naming clarity by rotation. At present, the application of factor analysis method in rockburst intensity level prediction is relatively small in order to eliminate the correlation between rockburst prediction indicators. This paper uses the factor analysis method to extract the characteristics of rockburst prediction indicators, using the original rockburst prediction indicators with minimal loss of information, with comprehensive rockburst indicators, as much as possible to reflect the original rockburst prediction indicators information, which is a good solution to the problem of overlapping information indicators.

Probabilistic neural networks (PNNs) were proposed by Dr. D. F. Specht in 1988 and can implement the functions of nonlinear learning algorithms using linear learning algorithms, with the advantages of simple structure, good expansion performance, fast convergence, and high fault tolerance [31]. However, when the probabilistic neural network is used, the problem of selecting the optimal smoothing factor is somewhat subjective and tedious. Therefore, this paper uses the sparrow search algorithm (SSA) to select the optimal smoothing factor, which has the advantages of being rapid and efficient when optimizing for a single objective and good merit-seeking ability and solves the problem of selecting the optimal smoothing factor very well.

Combining the above research, this paper selects 75 groups of typical rockburst case data, combines factor analysis method, sparrow search algorithm, and probabilistic neural network, and establishes a rockburst intensity level prediction method based on the FA-SSA-PNN model. The method has the advantages of simple logic, easy implementation, strong generalization ability of the model, high prediction accuracy, fast convergence, and

applicability to small samples, which can be used as a new method for rockburst intensity level prediction. The present research results provide an important basis for predicting the rockburst intensity level in advance and provide preparation time for rockburst disaster prevention and control, and the method in this paper can also provide a reference for other geological hazard prediction problems similar to rockburst disasters.

2. Methods

2.1. Factor Analysis (FA)

Factor analysis (FA), is a multivariate statistical analysis method that combines multiple variables (or samples) with intricate relationships into a smaller number of factors. The calculation process is as follows:

With n rockburst predictor variables $X_1, X_2, \ldots, X_n$, n rockburst prediction variables can be represented by m factors $F_1, F_2, \ldots, F_m$ and the product of an $A_{n\times m}$ order factor loading matrix plus a special factor $\varepsilon = (\varepsilon_1, \varepsilon_2, \ldots, \varepsilon_n)$ $(n \geq m)$, while the established mathematical model of factor analysis is: $X_n = A_{n\times m}F_m + \varepsilon_n$, i.e., Equation (1):

$$\begin{bmatrix} X_1 \\ X_2 \\ \vdots \\ X_n \end{bmatrix} = \begin{bmatrix} a_{11} & a_{12} & \cdots & a_{1m} \\ a_{21} & a_{22} & \cdots & a_{2m} \\ \vdots & \vdots & \ddots & \vdots \\ a_{n1} & a_{n2} & \cdots & a_{nm} \end{bmatrix} \begin{bmatrix} F_1 \\ F_2 \\ \vdots \\ F_m \end{bmatrix} + \begin{bmatrix} \varepsilon_1 \\ \varepsilon_2 \\ \vdots \\ \varepsilon_n \end{bmatrix}, \quad (1)$$

$F_1, F_2, \ldots,$ and F_m are m independent common factors. The matrix $A_{n\times m}$ is called the factor loading matrix. a_{nm} denotes the weight of the nth variable on the mth factor variable, which reflects the importance of the common factor on the variable, and is important for explaining the common factor. The special factors in the model have a small effect relative to the main factor F_m in Equation (1) and are neglected in the study. The steps of the factor analysis are as follows:

The raw data need to be normalized before factor analysis to eliminate the effect of order of magnitude on the calculated results. The normalized treatment in this paper is specified as follows:

$$\begin{cases} X_{ij}^* = \left(X_{ij}^* - X_{\min}\right)/(X_{\max} - X_{\min}) \\ X_{ij}^* = \left(X_{\max} - X_{ij}^*\right)/(X_{\max} - X_{\min}) \end{cases}, \quad (2)$$

Equation: $X_{\max}$ is the maximum value in the sample; $X_{\min}$ is the smallest value in the sample; $X_{ij}{}^*$ is the normalized data value of indicator X_{ij} in the sample, $i = 1, 2, \ldots, n$; $j = 1, 2, \ldots, m$.

After the normalized process, the factor loading matrix is calculated from the eigenvalues λ_i of the sample correlation matrix R, which is symmetric,

$$R = \begin{bmatrix} 1 & r_{21} & r_{31} & \cdots & r_{p1} \\ r_{21} & 1 & r_{21} & \cdots & r_{p2} \\ r_{31} & r_{32} & 1 & \vdots & r_{p3} \\ \vdots & \vdots & \vdots & \ddots & \vdots \\ r_{q1} & r_{q2} & r_{q3} & \cdots & 1 \end{bmatrix}, \quad (3)$$

Equation: r_{qp} is the correlation coefficient of the variable F_m with F_n.

$$r_{qp} = \frac{\operatorname{cov}(F_q F_p)}{\sqrt{D(F_q)\sqrt{D}(F_p)}}, \quad (4)$$

Equation: cov(F_q, F_p) is the covariance of F_q and F_p; $D(F_q)$ and $D(F_p)$ are the variances of F_q and F_p, respectively. The raw sample data have been normalized so that there is:

$$\left.\begin{array}{l} D(F_q) = D(F_p) = 1 \\ b_{ir} = a_{ir}\cos\theta + a_{ir}\sin\theta \\ r_{qp} = a_{qp} \end{array}\right\}. \tag{5}$$

From the above equation, a_{qp} can be regarded as the correlation coefficient between F_q and F_p, which also exactly indicates the degree of linear combination of X_m and F_m. λ_i (i = 1, 2, . . . , m) are all the characteristic roots of the sample correlation matrix R, finding all the characteristic root λ_i (i = 1, 2, . . . , m) of the sample correlation matrix R and the corresponding normalized eigenvectors U_i (i = 1, 2, . . . , m),

$$\lambda_1 \geq \lambda_2 \geq \cdots \lambda_m \geq 0, \tag{6}$$

The eigenvectors are used to form the eigenvector matrix $U = (U_1, U_2, \ldots, U_m)$, and the load matrix is derived from the characteristic root and eigenvectors A,

$$A = (\sqrt{\lambda_1}U_1, \sqrt{\lambda_2}U_2, \cdots, \sqrt{\lambda_m}U_m, \tag{7}$$

The first k column vectors of the loading matrix A are used as the factor loading matrix, and the cumulative contribution of the factors is required,

$$\frac{\sum_{i=1}^{k}\lambda_i}{\sum_{i=1}^{m}\lambda_i} \geq 85\%. \tag{8}$$

The maximum variance method was chosen to perform the common factor rotation, and the new loading matrix B was obtained by left multiplying the loading matrix A with the orthogonal matrix Γ,

$$[\Gamma] = \begin{bmatrix} \cos\theta & -\sin\theta \\ \sin\theta & \cos\theta \end{bmatrix}. \tag{9}$$

Let the elements of the ith row and jth column of B be b_{ij}, then we have:

$$\left.\begin{array}{l} b_{ir} = a_{ir}\cos\theta + a_{ir}\sin\theta \\ b_{ir} = a_{ir}\cos\theta + a_{ir}\sin\theta \end{array}\right\}, \tag{10}$$

where θ is the orthogonal rotation angle, i = (1, 2, . . . , p); r, j = (1, 2, . . . , n). After this transformation, the aim is to polarize the loading matrix and spread the factor contributions as much as possible, i.e., the ${b^2}_{ir}$, ${b^2}_{ig}$ 2 sets of data are required to be spread as much as possible, the degree of dispersion is expressed by the variance of the samples (V_1, V_2, . . . , V_n), and the total variance is required to be maximum, that is, the request:

$$G = V_1 + V_2 + \cdots + V_n = \max, \tag{11}$$

When the number of common factors is more than 2 (i.e., when m > 2), the orthogonal matrix Γ can generally only be obtained iteratively, and then a total of $C_m^2 = m(m-1)/2$ rotations are required, after which a second round of C_m^2 pairwise rotations can be performed, and so on until the variance converges to a certain limit and the rotation is stopped. The steps of factor analysis in this paper are shown in Figure 1.

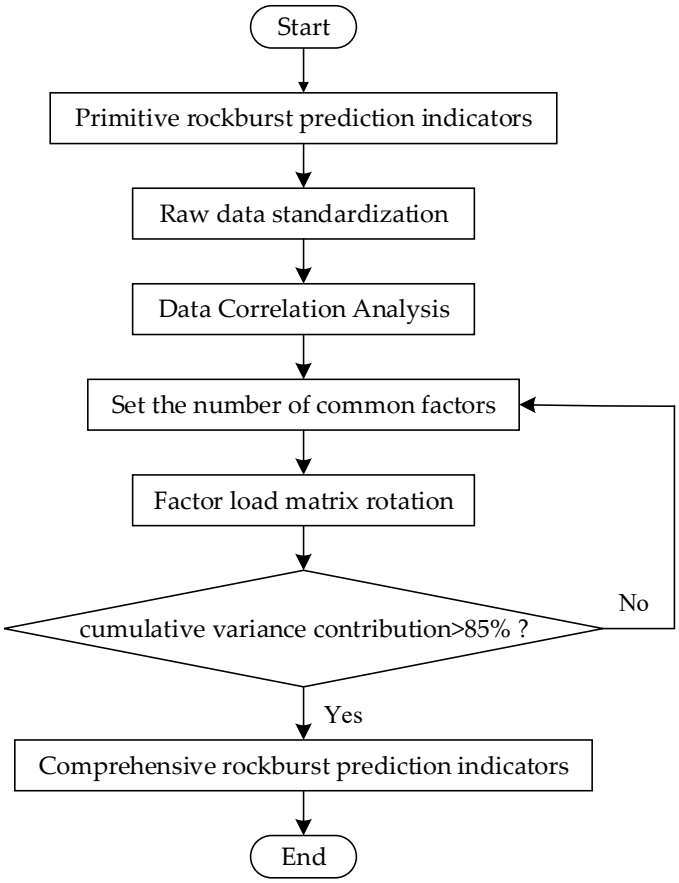

Figure 1. Factor analysis flow chart.

2.2. Sparrow Search Algorithm (SSA)

The Sparrow Search Algorithm [32] (SSA) is a new swarm intelligence optimization algorithm proposed in 2020 to simulate sparrow foraging and anti-predation behaviors, which divides the sparrows in the population into a discoverer, a follower, and a certain ratio of scouts. The finder is responsible for finding food, the follower joins the finder for foraging, and the scout is responsible for scouting the surrounding environment and alerting to the danger in time.

The sparrow as a discoverer has good adaptability. It will preferentially obtain food and provide foraging orientation for followers during foraging, and the location update of the discoverer in each iteration is described as in Equation (12):

$$\left.\begin{array}{l} x_{ij}^{t} \exp\left(\frac{-i}{\alpha \cdot iter_{\max}}\right), R_2 < ST \\ x_{ij}^{t} \exp\left(\frac{-i}{\alpha \cdot iter_{\max}}\right), R_2 < ST \end{array}\right\} = x_{ij}^{t+1}, \tag{12}$$

where t is the current number of iterations; L is an all-1 matrix of $1 \times d$; $iter_{\max}$ is the maximum number of iterations; Q and α are random numbers; x_{ij}^{t} denotes the position of the ith sparrow in the jth dimension at iteration t; R_2 and ST are the warning value and safety threshold. When $R_2 < ST$, it means there is no danger in the surrounding environment and the foraging range can continue to be expanded, and when $R_2 \geq ST$, it means the scout detects danger in the surrounding area and sends an alert to the population, telling the population to move to a safe area as soon as possible.

The updated description of the follower's location is as follows:

$$\left.\begin{array}{l} Q \exp\left(\frac{x_{wj}^{t} - x_{ij}^{t}}{i^2}\right), i > \frac{N}{2} \\ x_{pj}^{t+1} + \left| x_{ij}^{t} - x_{pj}^{t+1} \right| A^{+} L, other \end{array}\right\} = x_{ij}^{t+1}, \tag{13}$$

where A is a d-column matrix with random element values of 1 or -1 and $A^+ = A^T(AA^T)^{-1}$; x_{pj} is the optimal position of the discoverer; x_{wj} is the worst position in the game.

The scout generates the initial position randomly, and its subsequent position is updated as in Equation (14):

$$\left.\begin{array}{l} x_{ij}^t + \beta\left|x_{ij}^t - x_{bj}^t\right|, f_i > f_g \\ x_{ij}^t + K\frac{\left|x_{ij}^t - x_{WJ}^t\right|}{(f_i - f_w)+\varepsilon}, f_i = f_g \end{array}\right\} = x_{ij}^{t+1}, \quad (14)$$

where x_{bj} indicates the global best position; β denotes the iteration step size; f_i indicates the current level of adaptation; f_g and f_w denote the global optimal and worst adaptation degrees; K is a random number between $[-1, 1]$; ε is the smallest constant that prevents the denominator from going to zero.

After completing one round of iterations, as described above, the position of the population will be changed in some way, and each iteration will make the population change in the direction of better fitness, and finally the optimal fitness will be obtained.

2.3. Probabilistic Neural Network (PNN)

The Probabilistic Neural Network ((PNN)) [33,34] is a feed forward neural network based on radial basis neural network, which uses the Parzen window function to calculate the conditional probability density function of the samples to be recognized and then completes the classification and recognition of patterns by Bayes classification criterion, and its topology is shown in Figure 2.

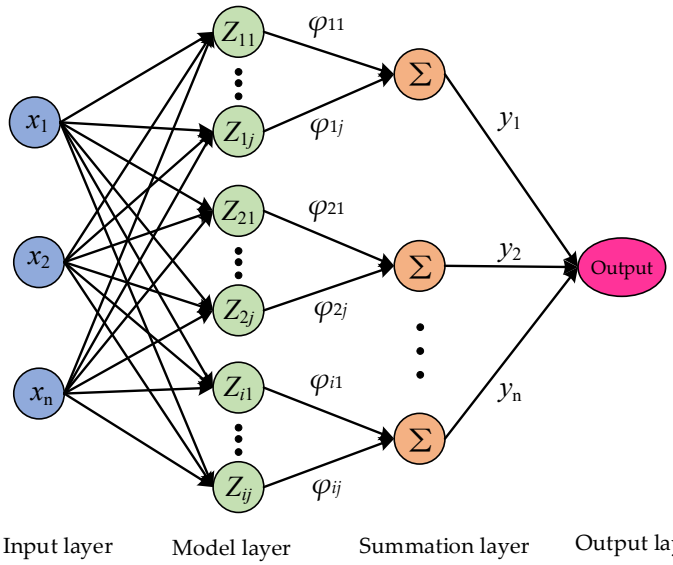

Figure 2. Topology of probabilistic neural network.

The role of the input layer is to receive the training sample data and multiply the values x of the input sample parameters with the weighting coefficients w_i to obtain the scalar product Z_i input to the model layer, as shown in Equation (15):

$$Z_i = xw_i, \quad (15)$$

The pattern layer is used to calculate the matching relationship between the input vector and each pattern and return a scalar value. The vector Z is input to the pattern layer,

and the input and output relationship of the jth neuron of the ith class of patterns in the pattern layer is:

$$\varphi_{ij} = \frac{1}{(2\pi)^{\frac{1}{2}}\sigma^d} exp\left[-(Z - Z_{ij})(Z - Z_{ij})\right]^{T/\sigma^2}, \quad (16)$$

where φ_{ij} is the output value of the jth neuron of the ith class of patterns in the pattern layer; σ is the smoothing factor; d is the dimensionality of the sample space data; and Z_{ij} is the jth center of the ith class of samples.

The main role of the summation layer is linear summation and weighted averaging. The summation layer takes the outputs of neurons belonging to the same class in the pattern layer and makes a weighted average,

$$v_i = \sum_{\mathrm{j}-1}^{L} \phi_{ij} \Big/ L, \quad (17)$$

where v_i is the output of class i, (i = 1, 2, . . . , n); n is the total number of training sample patterns; L denotes the number of neurons in class i.

The last layer is the output layer and the Bayesian classification rule is applied to the output of the summation layer, and the neuron with the maximum posterior probability density is found to have an output of 1 among all the output layer neurons, and the rest of the neurons have an output of 0,

$$y = \mathrm{argmax}(f_i), \quad (18)$$

where y indicates the output of the output layer.

3. Dataset Preparations

3.1. Selection of Rockburst Prediction Indicators

The rockburst mechanism is complex and has significant randomness and suddenness. The selection of indicators is the key to accurately predicting the rockburst. The selection of predictive indicators should meet the following conditions: (1) less influenced by external factors, so the actual measured values of indicators are easy to obtain; (2) has a good representative, so it can accurately reflect the main characteristics of the occurrence of rockbursts; (3) capable of reflecting comprehensive information on rockburst characteristics. This paper is based on a large number of rockburst case study analyses to determine the rockburst prediction evaluation indicators.

From the geological structure of the occurrence of rockbursts, rockbursts usually occur in the deeper buried underground works and higher structural stress in the rock mass. From the structural surface of the rock, rockburst often occurs near the hard structural surface, and the more irregular the structural surface, the more likely to occur rockburst. The maximum tangential stress in the surrounding rock can reflect the above factors well, so the maximum tangential stress in the surrounding rock (σ_θ) is selected as the rockburst prediction evaluation indicators.

The occurrence of rockburst section form of the surrounding rock is mainly tensile damage, and rockburst usually occurs in the structural integrity and hard rock. The hardness of the rock is usually expressed in terms of uniaxial compressive strength. Through reading a large amount of literature, we found that the actual rockburst case of uniaxial tensile strength and uniaxial compressive strength is more documented, and most of the rock projects need to obtain these two mechanical properties, so the uniaxial tensile strength (σ_t) and uniaxial compressive strength (σ_c) are rockburst prediction evaluation indicators.

From an energy point of view, rockburst is the rapid release of energy gathered in high-energy reservoirs. Under the same stress conditions, the elastic energy index, the performance of rock aggregation, and the release of energy is positively correlated, so the rock elastic energy index (W_et) is selected as the rockburst prediction indicators. A number of rockburst cases have shown that the occurrence of rockbursts is closely related to the

brittleness of the rock, and the brittleness coefficient of the rock is often used as a rockburst criterion. The stress coefficient is also commonly used as a rockburst criterion; therefore, the brittleness index (σ_c/σ_t) and the stress coefficient (σ_θ/σ_c) are rockburst prediction evaluation indicators.

Comprehensive analysis of the above, according to the causes and characteristics of the occurrence of rockburst, six rockburst impact factors (σ_θ, σ_t, σ_c, σ_c/σ_t, σ_θ/σ_c, W_{et}) were selected as the rockburst prediction indicators in this paper.

3.2. Sample Library of Rockburst Case Data

Rockburst is currently a common geological hazard in many underground rock projects at home and abroad, and many engineering rockburst cases have been well documented. In this paper, through literature research [35–38], based on the rockburst prediction evaluation indicators selected by the study, 75 groups of typical rockburst cases at home and abroad were selected, and some of the raw data are shown in Table 1, and the rockburst intensity level was divided into four levels, of which the actual distribution of rockburst levels is shown in Figure 3.

Table 1. Data of some domestic and international rockburst cases [35–38].

Serial Number	Primitive Rockburst Prediction Indicators						Comprehensive Rockburst Prediction Indicators			Actual Level
	σ_θ	σ_c	σ_t	σ_θ/σ_c	σ_c/σ_t	W_{et}	CPI_1	CPI_2	CPI_3	
1	18.8	178	5.7	0.11	31.23	7.4	0.549	0.456	0.964	I
2	96.41	18.32	0.38	0.19	47.93	1.87	0.411	0.657	0.933	I
3	15.2	53.8	5.56	0.283	9.68	1.92	0.562	0.314	1.001	I
...	...	...	...	...	...	...	...	...	...	...
61	48	120	1.5	0.4	80	5.8	0.606	0.998	0.746	III
62	48.75	180	8.3	0.27	21.69	5	0.634	0.320	0.768	III
63	105	115	1.5	0.55	76.67	5.7	0.538	0.895	0.486	III
64	33.94	117.48	4.23	0.29	27.77	2.37	0.644	0.497	0.892	II
65	14.96	115	5	0.1	23	5.7	0.498	0.403	1.059	I
66	157.3	91.23	6.92	0.58	13.18	6.27	0.311	0.088	0.317	IV
67	91.43	157.63	11.96	0.58	13.18	6.27	0.559	0.108	0.397	IV
68	13.9	124	4.22	0.112	29.4	2.04	0.667	0.538	1.086	I
69	38.2	71.4	3.4	0.53	21	3.6	0.539	0.423	0.718	III
70	39.4	69.2	2.7	0.57	25.6	3.8	0.537	0.478	0.686	III
71	52	175	7	0.3	25	5.2	0.615	0.368	0.744	III
72	105	304.21	20.9	0.35	14.56	10.57	0.639	−0.094	0.331	IV
73	35.82	127.93	4.43	0.28	28.9	3.67	0.608	0.485	0.872	II
74	69.8	198	22.4	0.35	8.84	4.68	0.763	−0.062	0.570	II
75	55.4	176	7.3	0.31	24.11	9.3	0.452	0.290	0.683	III

Note: Groups 1 to 60 are the training sets; Groups 61 to 75 are the test sets.

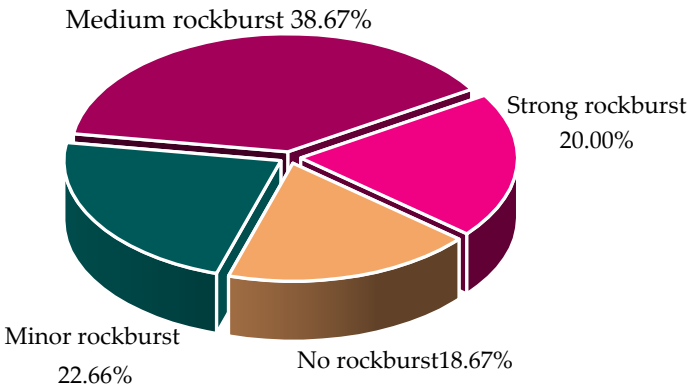

Figure 3. Rockburst actual intensity level distribution.

The number of rockburst case data collected in the least number of I samples, 14; the number of II samples is 17; the number of III samples is the most, 29; the number of IV samples is 15; the ratio of various types of samples is 1.4:1.7:2.9:1.5; there is a certain imbalance in the characteristics of various types of samples. However, the ratio of the maximum sample size to the minimum sample size is only slightly greater than 2. The imbalance problem of rockburst samples is small. Figure 4 shows the violin diagram of rockburst prediction evaluation indicators, whose horizontal coordinates indicate different rockburst levels, and vertical coordinates are rockburst prediction evaluation indicators. The violin chart is a combination of a box chart and a nuclear density chart, which gives a good indication of the shape of the distribution of the data. The white dot in the middle of the box line box indicates the median, the middle box line box indicates the interquartile range, the thin line extending from it represents the 95% confidence interval, and the outer shape is the nuclear density estimate.

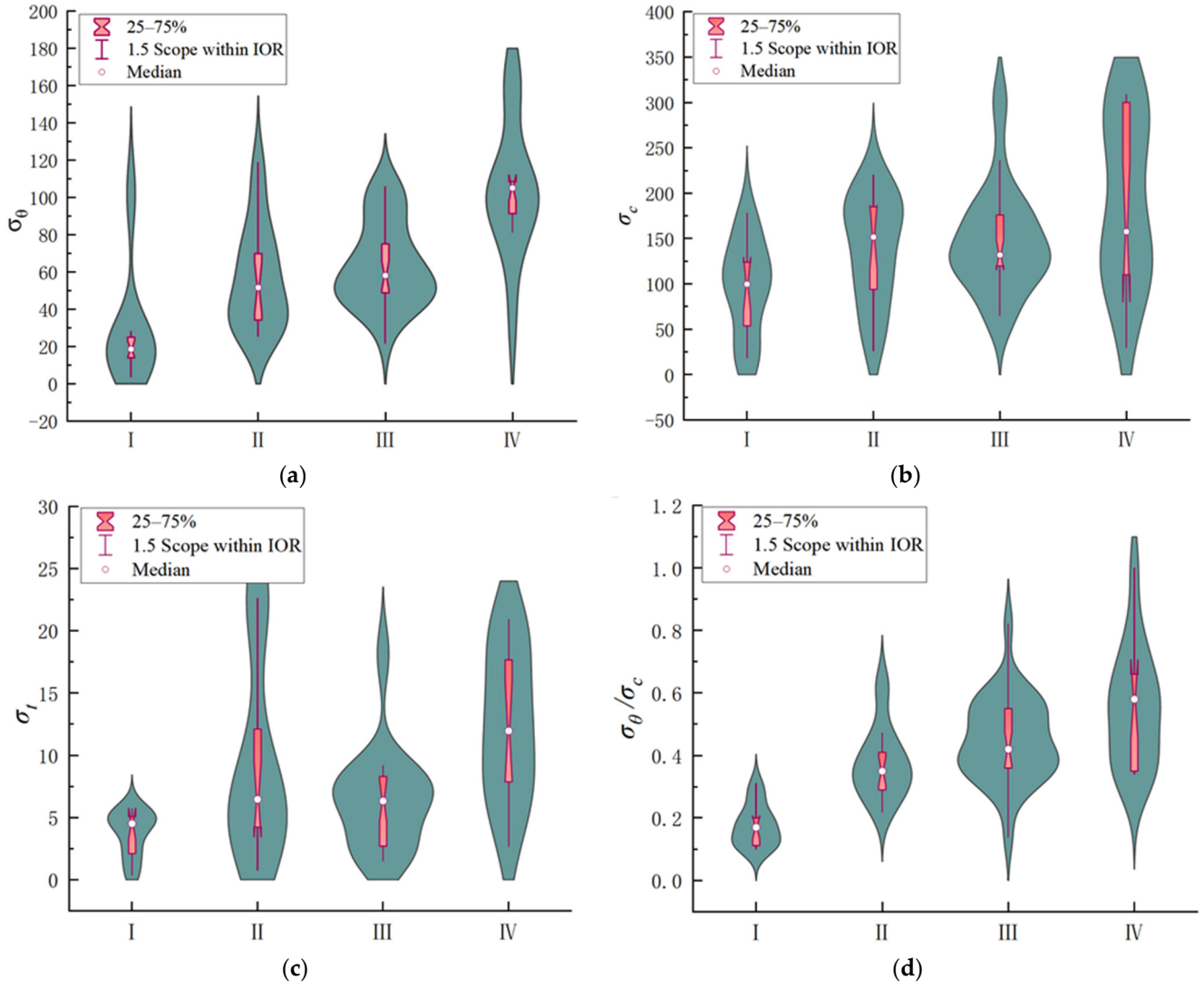

Figure 4. *Cont.*

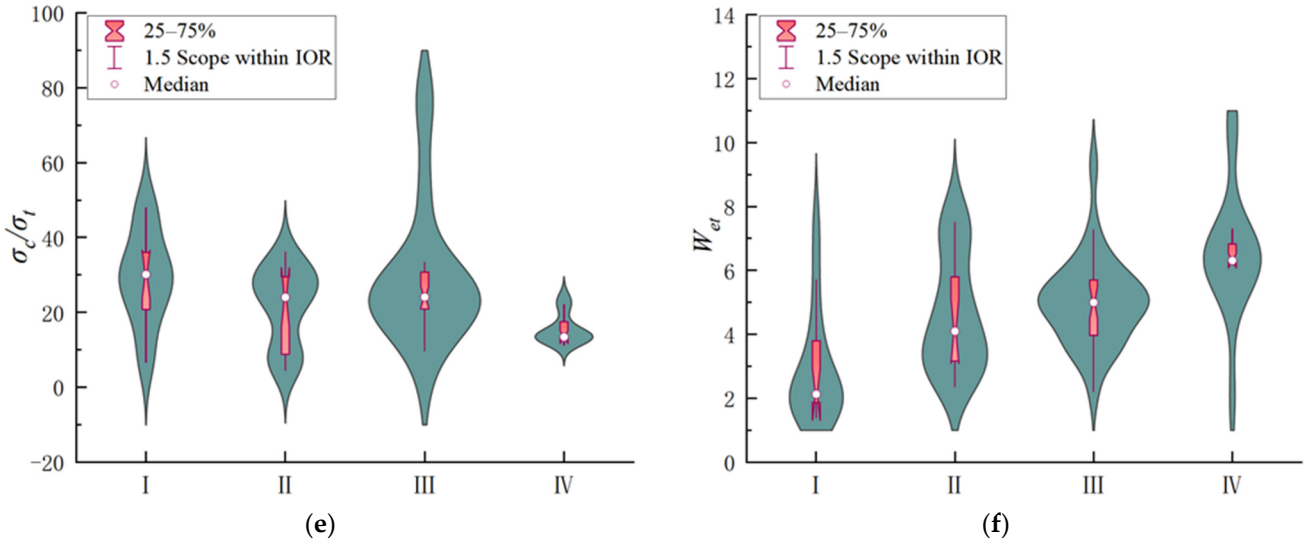

Figure 4. Violin diagram of rockburst prediction indicators: (**a**) σ_θ distribution; (**b**) σ_c distribution; (**c**) σ_t distribution; (**d**) σ_θ/σ_c distribution; (**e**) σ_c/σ_t distribution; (**f**) W_{et} distribution.

4. Implementation Process of FA-SSA-PNN Model

4.1. Model Construction Steps

The 75 groups of rockburst case data collected show that there is variability in the dimensionality, which in turn leads to a decrease in the accuracy of the rockburst prediction model. In order to eliminate the impact of the difference in the dimensionality between the indicators and improve the accuracy of the rockburst prediction model, it is necessary to reduce the original rockburst prediction data, the dimensionality of the resulting comprehensive rockburst prediction data into the rockburst prediction model, and the prediction results of the model for analysis and discussion.

In this paper, Matlab software to program the calculation of the neural network algorithm to establish the FA-SSA-PNN rockburst prediction model process is shown in Figure 5, and the main steps are as follows:

Step 1: Analysis of the impact of rockburst factors; the selection of rockburst prediction indicators.

Step 2: Collect rockburst case data according to the selected rockburst prediction indicators.

Step 3: Use factor analysis to reduce the dimensionality of the collected rockburst case data to obtain the comprehensive rockburst prediction index CPI_1, CPI_2, CPI_3.

Step 4: Partition the data set of the rockburst case data after dimensionality reduction processing; extract 80% of the overall rockburst prediction data samples as the training sets and 20% of the overall samples as the test sets.

Step 5: Imported the training samples into the SSA-PNN model and use the training for model training and updating parameters.

Step 6: After the training is completed, input the test samples to the model to test the network performance, get the rockburst intensity level prediction results, and calculate the accuracy of its rockburst intensity level prediction.

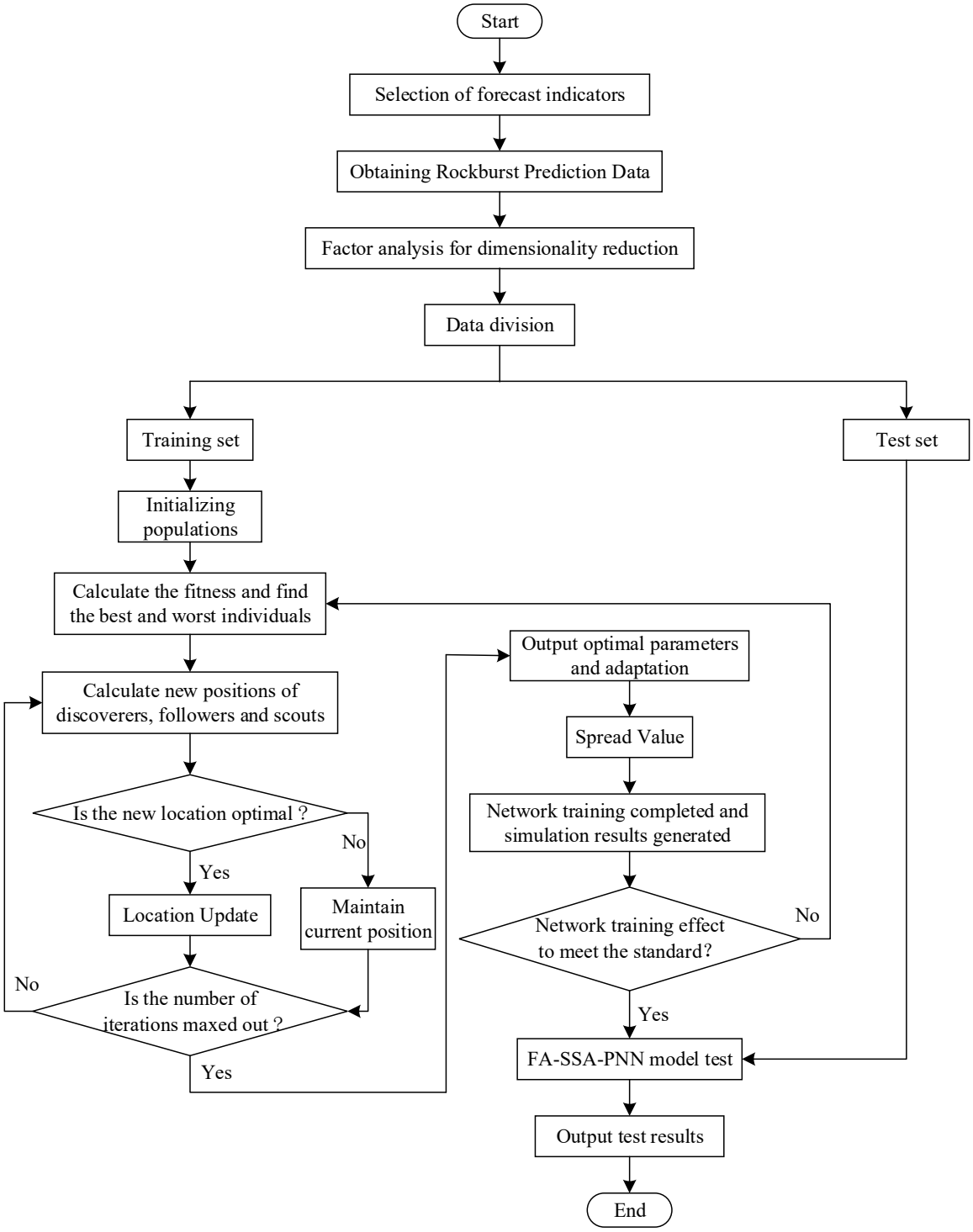

Figure 5. Flow chart of the rockburst prediction model of FA-SSA-PNN.

4.2. Test of Applicability of Factor Analysis

The rockburst cases at home and abroad were collected and organized, 75 groups of typical rockburst cases were selected as the sample data of the FA-SSA-PNN rockburst prediction model, the KMO test and Bartlett's spherical test were used to test the applicability of factor analysis on the sample data, and the test results and applicability test criteria are shown in Tables 2 and 3. It can be seen from Tables 2 and 3 that it is feasible to conduct factor analysis on the selected rockburst case data.

Table 2. Results of factor analysis method applicability test.

Kaiser-Meyer-Olkin test	KMO value	0.641
Bartlett spherical test	chi-squared test value	187.075
	Sig	0.000

Table 3. Applicability test criteria of factor analysis method.

Test Method	Range of Values	Factor Analysis Applicability
Kaiser-Meyer-Olkin test	>0.9	Perfect suitable
	0.8~0.9	Great suitable
	0.7~0.8	Relatively suitable
	0.6~0.7	Suitable
	0.5~0.6	Barely suitable
	<0.5	Not suitable
Bartlett spherical test	sig $\leq$ 0.01	Suitable

4.3. Data Processing

The absolute value of the correlation coefficient r reflects the degree of linear correlation between the two rockburst prediction evaluation indicators. When $|r| < 0.3$, it means that the correlation between the two rockburst prediction evaluation indicators is extremely weak and can be regarded as uncorrelated; when $0.3 < |r| < 0.5$, the two rockburst prediction evaluation indicators are low correlated; when $0.5 < |r| < 0.8$, the two rockburst prediction evaluation indicators are significantly correlated; when $0.8 < |r| < 1$, the two rockburst prediction evaluation indicators are extremely correlated. Correlation analysis of rockburst prediction evaluation indicators and the correlation coefficient between predictors is shown in Table 4. The absolute values of the correlation coefficients between σ_θ and σ_c, σ_θ and σ_t, σ_θ and σ_θ/σ_c, σ_c and σ_t, σ_c and W_{et}, and σ_t and σ_c/σ_t were all greater than 0.5, indicating that the rockburst prediction evaluation indicators were significantly correlated with each other and the sample data were suitable for factor analysis.

Table 4. Correlation coefficients among prediction evaluation indicators.

Indicators	σ_θ	σ_c	σ_t	σ_θ/σ_c	σ_c/σ_t	W_{et}
σ_θ	1.00	0.411	0.449	0.410	−0.114	0.541
σ_c	0.411	1.00	0.677	−0.089	−0.153	0.643
σ_t	0.449	0.677	1.00	0.142	−0.583	0.588
σ_θ/σ_c	0.410	−0.089	0.142	1.00	−0.220	0.276
σ_c/σ_t	−0.114	−0.153	−0.583	−0.220	1.00	−0.174
W_{et}	0.541	0.643	0.588	0.240	−0.174	1.00

Factor analysis was used to reduce the dimensionality of the standardized 75 sets of rockburst data, and Mardia gave the correspondence between the original number of variables and the number of principal factors after dimensionality reduction in Table 5. In this paper, 6 rockburst prediction evaluation indicators were selected as the original number of variables, so the number of principal factors after factor analysis was set to 3. Table 6 shows the total variance interpretation of the rockburst prediction evaluation indicators, and we can see that the eigen values of the first three factor variables are all greater than 1 and the cumulative contribution of the first three principal factors is 85.538% > 85%, indicating that the first three principal factors retain 85.538% of the information carried by the original variables, so the extraction of the first three principal factors as influencing factors is consistent with the previous setting.

Table 5. Relationship between the number of original variables and the number of main factors.

Number of original variables	5	7	8	9	11
Number of principal factors	2	3	4	5	6

Table 6. Total variance explained.

Principal Factor	**Load Sum of Squares**			**Sum of Squared Rotating Loads**		
	Eigen Value	**Variance Contribution**	**Cumulative Variance Contribution**	**Eigen Value**	**Variance Contribution**	**Cumulative Variance Contribution**
F_1	2.897	48.282%	48.282%	2.410	40.160%	40.160%
F_2	1.186	19.769%	68.051%	1.367	22.785%	62.945%
F_3	1.049	17.486%	85.538%	1.356	22.593%	85.538%

The changes in factor loadings before and after rotation are shown in Table 7. Combining the positive and negative correlations and the composite rate, it can be seen that the principal factor F_1 is significantly positively correlated with the rockburst prediction evaluation indicators σ_θ, σ_c, σ_t, σ_θ/σ_c, indicating that the principal factor F_1 concentrates on the maximum tangential stress, compressive strength, compressive strength, and the influence of the stress coefficient on the prediction results of rockburst. The principal factor F_2 is only positively correlated with the indicator σ_c/σ_t, indicating that the main factor F_2 combines the information of the indicators of the brittleness index, which can be referred to as the brittleness factor. The main factor F_3 is positively correlated with the indicator W_{et} only and can be referred to as the energy factor.

Table 7. Changes in factor loadings before and after rotation.

Indicators	**Factor Loading before Rotation**			**Factor Loadings after Rotation**		
	F_1	F_2	F_3	F_1	F_2	F_3
σ_θ	0.874	−0.150	−0.315	0.907	−0.130	−0.173
σ_c	0.823	−0.100	0.281	0833	−0.072	0.260
σ_t	0.769	−0.512	0.126	0.704	−0.622	0.570
σ_θ/σ_c	0.712	0.278	0.423	0.628	0.460	−0.606
σ_c/σ_t	0.344	0.875	0.123	−0.061	0.965	−0.118
W_{et}	0.489	−0.221	0.813	−0.029	−0.158	0.934

Table 8 shows the factor score coefficient matrix. The factor analysis reallocated the weights of the impact of rockburst prediction evaluation indicators on the principal factor and reduced the impact of poorly correlated rockburst prediction evaluation indicators on the principal factor, resulting in a functional expression between the principal factors Y_1, Y_2, Y_3 and the six rockburst prediction evaluation indicators, as follows (x_i^* is the standardized data value of x_i).

$$\left.\begin{array}{l} Y_1 = 0.243x_1^* + 0.444x_2^* + 0.212x_3^* - 0.166x_4^* + 0.185x_5^* + 0.363x_6^* \\ Y_2 = 0.227x_1^* + 0.061x_2^* - 0.376x_3^* - 0.050x_4^* + 0.793x_5^* + 0.136x_6^* \\ Y_3 = 0.409x_1^* - 0.266x_2^* - 0.103x_3^* - 0.736x_4^* + 0.006x_5^* + 0.095x_6^* \end{array}\right\}, \quad (19)$$

Table 8. Factor score coefficient matrix.

Indicators	Factor Score Coefficients		
	F_1	F_2	F_3
σ_θ	0.243	0.227	0.409
σ_c	0.444	0.061	−0.266
σ_t	0.212	−0.376	−0.103
σ_θ/σ_c	−0.166	−0.050	0.736
σ_c/σ_t	0.185	0.793	0.006
W_{et}	0.363	0.136	0.095

Standardized data are substituted into Equations (17)–(19) to obtain partial principal factor data (Table 1). The principal factor retains most of the information in the original data, so the three principal factors are comprehensive rockburst prediction evaluation indicators CPI_1, CPI_2, CPI_3.

4.4. Datasets Segmentation

The sample data of rockburst after factor analysis (see Table 1) were divided into datasets, and 20% of the 75 sets of rockburst case data were taken as the test set, while 80% of the remaining data were used as the training set of the neural network model. After the division, there were 60 sets of sample data in the training set, and the training set was used to train the neural network model and update the parameters. There were 15 sets of sample data in the test set, and the test set was used to evaluate the generalization ability of the model and test the real prediction accuracy of the model.

4.5. Model Parameter Setting and Implementation

The traditional PNN model uses the original rockburst prediction evaluation indicators (σ_θ, σ_t, σ_c, σ_c/σ_t, σ_θ/σ_c, W_{et}) as the input vectors of the model. The FA-SAA-PNN rockburst prediction model developed in this paper used factor analysis to preprocess the original rockburst prediction evaluation indicators, and the comprehensive rockburst prediction indicators CPI_1, CPI_2, CPI_3 obtained after factor analysis were used as the prediction input vectors of the model. The selection of the smoothing factor is the key to the performance of PNN networks, and when the value of the smoothing factor is too small, it tends to cause the network to be overfitted and in essence a nearest neighbor classifier; when the value of the smoothing factor is too large, the details cannot be fully distinguished so close to a linear classifier [39]. This paper makes use of the good global search ability of the SSA algorithm to optimize the smooth factor of PNN neural network. The algorithm has the advantages of being rapid and efficient when optimizing for a single objective, as well as good merit-seeking ability, which solves the problem of selecting the optimal smoothing factor and improves the accuracy of the prediction model.

At present, there is no uniform standard for rockburst intensity grading, and scholars have recognized the rockburst intensity level in four classes, respectively: no rockburst (I), minor rockburst (II), medium rockburst (III), and strong rockburst (IV). This paper uses the PNN network model output vector set to 1×4 line vector, the i class in the line vector of the i neuron output value of 1, and the rest of the neuron output value of 0, such as the output vector is (0, 0, 1, 0), which means that the prediction model predicts the sample data as a medium rockburst (III).

The main parameters of the FA-SSA-PNN model are shown in Table 9, and the rockburst prediction model is programmed and calculated in this paper using Matlab software version 2018b, and the code implementation is based on M language.

Table 9. Main parameters of FA-SSA-PNN model.

Serial Number	Parameters	Parameter Values
1	Number of neurons in the input layer	3
2	Number of neurons in the pattern layer	60
3	Number of neurons in summation layer	4
4	Number of neurons in the output layer	4
5	Mode layer activation function	Gauss function
6	Optimization parameters	Spread Value
7	Number of populations of SSA	100
8	Maximum number of iterations of SSA	20
9	Proportion of discoverers	70%
10	Scout's ratio	20%
11	Early warning values	0.6

5. Model Performance Evaluation and Comparison

To verify the merit of the FA-SSA-PNN rockburst prediction model, test samples were input into the FA-SSA-PNN model, FA-PNN model, PNN model, RF model, SVM model, and ANN model [39], and the prediction results of each model are shown in Figure 6. To comprehensively evaluate the classification performance of each model, F_1 value (the summed average of precision and recall), macro-average F_1 value (the arithmetic mean of F_1 for each category), and accuracy rate are used as the evaluation indicators of the models in this paper. F_1 value and macro-average F_1 value reflect the classification performance of the models for different rockburst intensity levels, and accuracy rate reflects the overall classification performance of the models.

The evaluation indicators for the six rockburst prediction models are shown in Table 10, and a comparison of the models shows that:

(1) The FA-SSA-PNN model does not improve the F_1 value of the primary rockburst compared to the PNN model; the F_1 value for Level 2 rockburst is increased by 50% (from 50% to 100%); the F_1 value for Level 3 rockburst is increased by 25.6% (from 66.7% to 92.3%); and the F_1 value for Level 4 rockburst is increased by 20% (from 80% to 100%).

(2) Compared with the original PNN model, the macro-average F_1 value reflecting the classification performance of the model for different rockburst intensity level increased by 18.9% (from 69.2% to 88.1%) after the introduction of FA dimensionality reduction, and the macro-average F_1 value improved but remained low, and then, after the optimization of the PNN neural network by the SSA algorithm, the macro-average F_1 value increased by another 5% (from 88.1% to 93.1%), and the macro-average F_1 values of the FA-SSA-PNN model were significantly higher than those of the other five rockburst prediction models.

(3) The accuracy of the FA-PNN model after the introduction of FA improved by 13.3% (from 66.7% to 80%) compared with the original PNN model, and then, after the optimization of the PNN neural network by the SSA algorithm, the accuracy of the model improved by another 13.3% (from 80% to 93.3%), and the prediction accuracy of the FA-SSA-PNNN model was significantly higher than that of the other models, verifying the advantages and disadvantages of the FA-SSA-PNN rockburst intensity level prediction model.

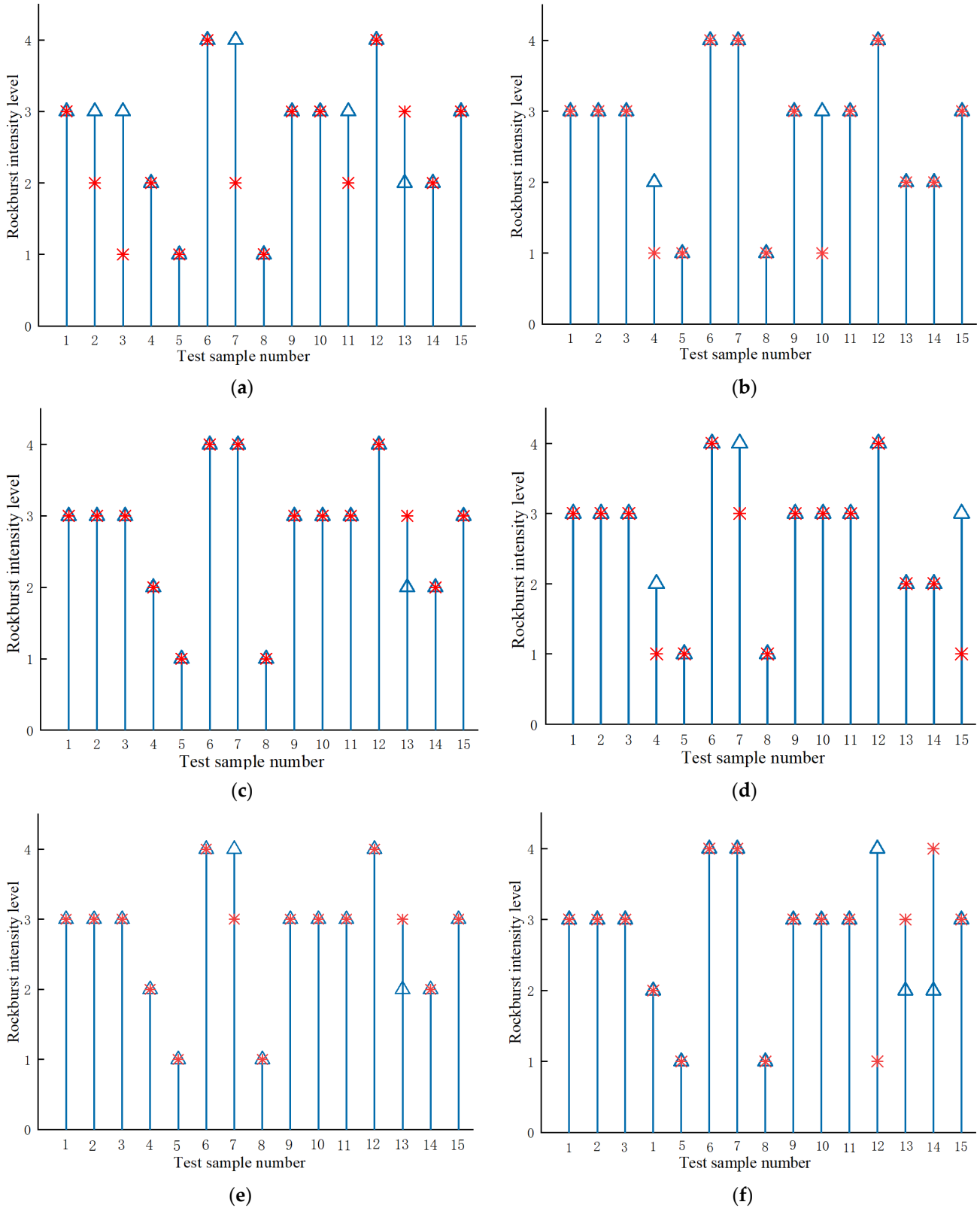

Figure 6. Rockburst prediction model test results: (**a**) PNN model; (**b**) FA-PNN model; (**c**) FA-SSA-PNN model; (**d**) ANN model; (**e**) SVM model; (**f**) RF model.

Table 10. Model evaluation indicators.

Evaluation Indicators	Intensity Level	PNN	FA-PNN	SSA-FA-PNN	ANN	SVM	RF
Accuracy rate	I	0.667	0.500	0.667	0.500	1.000	0.667
	II	0.400	1.000	1.000	1.000	1.000	1.000
	III	0.800	1.000	1.000	0.857	0.778	0.875
	IV	1.000	1.000	1.000	1.000	1.000	0.667
Recall Rate	I	1.000	1.000	1.000	1.000	1.000	1.000
	II	0.667	0.667	1.000	0.667	0.667	0.333
	III	0.571	0.857	0.857	0.857	1.000	1.000
	IV	0.667	1.000	1.00	0.800	0.667	0.667
F_1 value	I	0.800	0.667	0.80	0.667	1.000	0.800
	II	0.500	0.800	1.00	0.800	0.800	0.500
	III	0.667	0.923	0.923	0.857	0.875	0.933
	IV	0.80	1.000	1.00	0.667	0.800	0.667
Macro average F_1 value	-	0.692	0.881	0.931	0.781	0.86.9	0.725
Accuracy	-	0.667	0.800	0.933	0.800	0.800	0.867

6. Conclusions

As more and more underground rock projects move deeper at an unprecedented rate, the geological environment in which the rock masses are embedded is more complex, and the problem of rockburst hazards is becoming increasingly prominent. In this paper, based on 75 sets of typical rockburst case data collected, a rockburst intensity level prediction model based on FA-SSA-PNN is established, and F_1 value, macro-averaged F_1 value, and accuracy rate are introduced as the evaluation indexes of rockburst prediction model classification performance. This study proposes a new method for predicting the intensity level of rockbursts, which provides better guidance for the problem of predicting rockbursts in deep underground rock projects and can provide a reference for other geological hazard prediction problems similar to rockburst hazards, with the following main conclusions:

(1) The maximum tangentialstress of surrounding rock (σ_θ), uniaxial tensile strength (σ_t), uniaxial compressive strength (σ_c), brittleness index (σ_c/σ_t), stress coefficient (σ_θ/σ_c), and elastic energy index (W_{et}) of surrounding rock are selected to form a rockburst prediction index system. The characteristic information of the original rockburst prediction indexes was compressed and extracted by the factor analysis method, and three comprehensive rockburst prediction indexes, CPI_1,CPI_2, and CPI_3, were obtained. The introduction of factor analysis into the rockburst intensity level prediction eliminates the correlation between indicators and solves the problem of overlapping information of indicators, so that the comprehensive prediction index of rockburst after dimensionality reduction has a broader mathematical expression of Gaussian function in the PNN model.

(2) Fifteen sets of rockburst case data were sampled as test data, and the prediction results of the FA-PNN model were analyzed and compared with those of the original PNN model. It was found that the macro-average F_1 value and accuracy of the FA-PNN model were improved, with the macro-average F_1 value reaching 88.1% (from 69.6% to 88.1%) and the accuracy rate reaching 80% (from 66.7% to 80%).

(3) The SSA algorithm was used to select the smoothing factors in PNN to avoid the subjectivity and contingency of the existence of artificial preset smoothing factors. The comparison between the prediction results of FA-SSA-PNN rockburst prediction model and those of FA-PNN rockburst prediction model shows that, after the introduction of SSA algorithm, the accuracy of FA-SSA-PNN rockburst prediction model significantly improved, reaching 93.3% (increased from 80% to 93.3%), and the macro-average F_1 value is 93.1% (increased from 88.1% to 93.1%). Moreover, the SSA algorithm has good optimization ability and can complete the optimization of

smoothing factors in a few seconds. It greatly reduces the operation time of the model and improves the prediction efficiency of the model.

(4) The prediction results of the FA-SSA-PNN model were compared and analyzed with those of the FA-PNN model, PNN model, RF model, SVM model, and ANN model, and the results showed that the macro-averaged F_1 values and the prediction accuracy of the FA-SSA-PNN model were significantly higher than those of the other five models, which verified the feasibility and effectiveness of the FA-SSA-PNN rockburst prediction model.

The complexity of the rockburst mechanism and the many factors that induce rockburst, such as the traditional rockburst prediction methods, have not been able to make accurate and efficient predictions of the rockburst intensity level. Therefore, it will become more and more important to propose new methods for predicting rockburst intensity levels.

Author Contributions: Conceptualization, G.X. and K.L.; methodology, G.X.; software, G.X.; validation, Q.Q. and M.L.; formal analysis, G.X.; resources, R.Y.; data curation, G.X. and M.L.; writing—original draft preparation, G.X.; writing—review and editing, K.L. and Q.Q., supervision M.L. and R.Y.; visualization, Q.Q. and M.L.; supervision, R.Y.; project administration, Q.Q.; funding acquisition, K.L. All authors have read and agreed to the published version of the manuscript.

Funding: This research was supported by the National Natural Science Foundation of China (Grant No. 51934003) and the Yunnan major scientific and technological special project (Grant No. 202102AG050024).

Data Availability Statement: No applicable.

Conflicts of Interest: The authors declare no conflict of interest.

References

1. Feng, X.; Xiao, Y.; Feng, G.; Yao, Z.; Chen, B.; Yang, C.; Su, G. Study on the development process of rockbursts. *Chin. J. Rock Mech. Eng.* **2019**, *38*, 649–673. [CrossRef]
2. He, S.; Song, D.; Li, Z.; He, X.; Chen, J.; Li, D.; Tian, X. Precursor of Spatio-temporal Evolution Law of MS and AE Activities for Rock Burst Warning in Steeply Inclined and Extremely Thick Coal Seams Under Caving Mining Conditions. *Rock Mech. Rock Eng.* **2019**, *52*, 2415–2435. [CrossRef]
3. Xue, Y.; Li, Z.; Li, S.; Qiu, D.; Tao, Y.; Wang, L.; Yang, W.; Zhang, K. Prediction of rock burst in underground caverns based on rough set and extensible comprehensive evaluation. *Bull. Eng. Geol. Environ.* **2019**, *78*, 417–429. [CrossRef]
4. Li, X.; Gong, F.; Wang, S.; Li, D.; Tao, M.; Zhou, J.; Huang, L.; Ma, C.; Du, K.; Feng, F. Coupled static-dynamic loading mechanical mechanism and dynamic criterion of rockburst in deep hard rock mines. *Chin. J. Rock Mech. Eng.* **2019**, *38*, 708–723. [CrossRef]
5. Lin, M.; Gao, C.; Xia, Y.; Zhang, D.; Liu, X.; Liang, X. Rock burst initiation and precursors in a model specimen based on acoustic emission and infrared monitoring. *Arab. J. Geosci.* **2022**, *15*, 333. [CrossRef]
6. Ren, J.; Zhang, W.; Wu, Z.; Li, J.; Shen, Y. Microseismic Signals in Heading Face of Tengdong Coal Mine and Their Application for Rock Burst Monitoring. *Shock. Vib.* **2021**, *2021*, 6650446. [CrossRef]
7. Shirani Faradonbeh, R.; Shaffiee Haghshenas, S.; Taheri, A.; Mikaei, R. Application of self-organizing map and fuzzy c-mean techniques for rockburst clustering in deep underground projects. *Neural Comput. Appl.* **2019**, *32*, 8545–8559. [CrossRef]
8. Ma, C.; Chen, W.; Tan, X.; Tian, H.; Yang, J.; Yu, J. Novel rockburst criterion based on the TBM tunnel construction of the Neelum–Jhelum (NJ) hydroelectric project in Pakistan. *Tunn. Undergr. Space Technol.* **2018**, *81*, 391–402. [CrossRef]
9. Xu, L.; Wang, L. Study on the laws of rockburst and its forecasting in the tunnel of Erlang Mountain road. *Chin. J. Geotech. Eng.* **1999**, *21*, 569–572.
10. Lu, J. Study on mechanism of rockburst in a headrace tunnel. In *1st National Congress of Chinese Society for Numerical Calculation and Model Experiment of Rock Mechanics*; Southwest Jiaotong University Press: Chengdu, China, 1986; pp. 210–214.
11. Jiang, L.; Kong, P.; Zhang, P.; Shu, J.; Wang, Q.; Chen, L.; Wu, Q. Dynamic Analysis of the Rock Burst Potential of a Longwall Panel Intersecting with a Fault. *Rock Mech. Rock Eng.* **2019**, *53*, 1737–1754. [CrossRef]
12. Yang, Z.; Liu, C.; Zhu, H.; Xie, F.; Dou, L.; Chen, J. Mechanism of rock burst caused by fracture of key strata during irregular working face mining and its prevention methods. *Int. J. Min. Sci. Technol.* **2019**, *29*, 889–897. [CrossRef]
13. Ma, T.; Tang, C.; Tang, S.; Kuang, L.; Yu, Q.; Kong, D.; Zhu, X. Rockburst mechanism and prediction based on microseismic monitoring. *Int. J. Rock Mech. Min. Sci.* **2018**, *110*, 177–188. [CrossRef]
14. Xu, C.; Liu, X.; Wang, E.; Zhang, Y.; Wang, S. Rockburst prediction and classification based on the idealpoint method of information theory. *Tunn. Undergr. Space Technol.* **2018**, *81*, 382–390. [CrossRef]
15. Guo, J.; Zhang, W.; Zhao, Y. A multidimensional cloud model for rockburst prediction. *Chin. J. Rock Mech. Eng.* **2018**, *37*, 1199–1206. [CrossRef]

16. Lin, Y.; Zhou, K.; Li, J. Application of cloud model in rock burst prediction and performance comparison with three machine learnings algorithms. *IEEE Access* **2018**, *30*, 958–968. [CrossRef]
17. Wang, X.; Li, S.; Xu, Z.; Xue, Y.; Hu, J.; Li, Z.; Zhang, B. An interval fuzzy comprehensive assessment method for rock burst in underground caverns and its engineering application. *Bull. Eng. Geol. Environ.* **2019**, *78*, 5161–5176. [CrossRef]
18. Adoko, A.; Gokceoglu, C.; Wu, L.; Zuo, Q. Knowledge-based and data-driven fuzzy modeling for rockburst prediction. *Int. J. Rock Mech. Min. Sci.* **2013**, *61*, 86–95. [CrossRef]
19. Wang, C.; Wu, A.; Lu, H.; Bao, T.; Liu, X. Predicting rockburst tendency based on fuzzy matter–element model. *Int. J. Rock Mech. Min. Sci.* **2015**, *75*, 224–232. [CrossRef]
20. Shi, X.; Zhou, J.; Dong, L.; Hu, H.; Wang, H.; Chen, S. Application of unascertained measurement model to prediction of classification of rock burst Intensity. *Chin. J. Rock Mech. Eng.* **2010**, *29*, 2720–2726.
21. Li, Z.; Xue, Y.; Li, S.; Qiu, D.; Zhang, L.; Zhou, Y.; Zhou, B. Rock burst risk assessment in deep-buried underground caverns: A novel analysis method. *Arab. J. Geosci.* **2020**, *13*, 388. [CrossRef]
22. Peng, T.; Deng, H. Comprehensive evaluation on water resource carrying capacity in karst areas using cloud model with combination weighting method: A case study of Guiyang, southwest China. *Environ. Sci. Pollut. Res.* **2020**, *27*, 37057–37073. [CrossRef] [PubMed]
23. Gong, F.; Li, X. Distance discrimination method for rockburst occurrence and intensity classification prediction and its application. *Chin. J. Rock Mech. Eng.* **2007**, *26*, 1012–1018.
24. Yang, X.; Pei, Y.; Cheng, H.; Hou, X.; Lu, J. Prediction method of rockburst intensity grade based on SOFM neural network model. *Chin. J. Rock Mech. Eng.* **2021**, *40*, 2708–2715. [CrossRef]
25. Li, M.; Li, K.; Qin, Q.; Wu, S.; Liu, Y.; Liu, B. Discussion and selection of machine learning algorithm model for rockburst intensity grade prediction. *Chin. J. Rock Mech. Eng.* **2021**, *40*, 2806–2816. [CrossRef]
26. Tang, Z.; Xu, Q. Rockburst prediction based on nine machine learning algorithms. *Chin. J. Rock Mech. Eng.* **2020**, *39*, 773–781. [CrossRef]
27. Tian, R.; Meng, H.; Chen, S.; Wang, C.; Zhang, F. Prediction of intensity classification of rockburst based on deep neural network. *J. Chin. Coal. Soc.* **2020**, *45*, 191–201. [CrossRef]
28. Jia, Y.; Lu, Q.; Shang, Y. Rockburst prediction using particle swarm optimization and generalized regression neural network. *Chin. J. Rock Mech. Eng.* **2013**, *32*, 343–348.
29. Xue, Y.; Bai, C.; Qiu, D.; Kong, F.; Li, Z. Predicting rockburst with database using particle swarm optimization and extreme learning machine. *Tunn. Undergr. Space Technol.* **2020**, *98*, 103287. [CrossRef]
30. Zhou, J.; He, Y.; Huang, R.; Ju, N. Weights of slope stability evaluation indexes based on factor analysis method. *J. Southwest Jiaotong Univ.* **2015**, *50*, 325–330.
31. Wu, S.; Zhang, C.; Cheng, Z. Prediction of intensity classification of rockburst based on PCA-PNN principle. *J. Chin. Coal Soc.* **2019**, *44*, 2767–2776. [CrossRef]
32. Chen, Y.; Liu, Z.; Xiao, C.; Zhao, X.; Li, K.; Pang, L.; Shi, Y.; Li, S. Overlapping Peak Analysis of Soil Heavy Mettal X-Ray Fluorescence Spectra Based on Sparrow Search algorithm. *Spectrosc. Spectr. Anal.* **2021**, *41*, 2175–2180.
33. Cheng, B. Research on Transformer Fault Diagnosis Based on the Combination of Rough Set-Probabilistic Neural Network. Master's Thesis, Guangxi University, Nanning, China, 2008.
34. Du, Z.; Zhao, J.; Li, H.; Zhang, X. Afauit diagnosis method of a plunger pump based on SA-EMD-PNN. *J. Shock Vib.* **2019**, *38*, 145–152. [CrossRef]
35. Wang, Y.; Li, W.; Li, Q.; Xu, Y.; Tan, G. Method of fuzzy comprehensive evaluations for rockburst prediction. *Chin. J. Rock Mech. Eng.* **1998**, *17*, 493–501.
36. Zhou, J.; Li, X.; Shi, X. Long-term prediction model of rockburst in underground openings using heuristic algorithms and support vector machines. *Saf. Sci.* **2011**, *50*, 629–644. [CrossRef]
37. Dong, L.; Li, X.; Peng, K. Prediction of rockburst classifi-cation using Random Forest. *Trans. Nonferrous Met. Soc. China* **2013**, *23*, 472–477. [CrossRef]
38. Afraei, S.; Shahriar, K.; Madani, S. Developing intelligent classification models for rock burst prediction after recognizing significant predictor variables, Section 1: Literature review and data preprocessing procedure. *Tunn. Undergr. Space Technol.* **2019**, *83*, 324–353. [CrossRef]
39. Wang, J.; Zhou, Z.; Li, K.; Wang, H.; Fu, Z.; Li, X. Evaluation model for the risk grade of rock burst based on the R-type factor analysis and a probabilistic neural network. *J. Shock Vib.* **2019**, *38*, 192–203. [CrossRef]